AIAA JOURNAL
Vol. 37, No. 4, April 1999

Modeling of Spacecraft Rarefied Environments Using a Proposed Surface Model

Virendra K. Dogra*
John Hopkins University, Applied Physics Laboratory, Laurel, Maryland 20723-6099
Robert J. Collins†
University of Minnesota, Minneapolis, Minnesota 55455
and
Deborah A. Levin‡
George Washington University, Washington, D.C. 20052

The modeling of spacecraft glow surrounding a small clean satellite is discussed. A direct simulation Monte Carlo (DSMC) technique was used to model the flowfield and included both surface and gas-phase chemical reactions. It has been suggested that emission from excited NO_2 molecules produces the spacecraft glow. The DSMC calculations included chemical reactions in the flowfield to produce NO, as well as surface chemical reactions to generate the NO_2. The orbit-dependent optical radiation was calculated and compared with data from the Atmosphere Explorer experiment over the 140–200-km altitude range. The results show that the surface model can account for the observed data in magnitude and altitude dependence for suitable choices of the surface heat of absorption and freestream NO concentration.

Introduction

SPACECRAFT-INDUCED glow observations and measurements of the Atmosphere Explorer and the Space Shuttle[1,2] show qualitative similarity in the spectral features of both data sets despite the different environments. Various models have been suggested to explain the Shuttle glow observations,[3–7] which were made in the environment of a large spacecraft. The environment of large spacecraft is generally contaminated by hydrazine rocket engines used for orbit-keeping purposes and other outgassing processes. The clean environment of a small spacecraft makes it a better candidate for modeling the glow and comparing with data. The model was developed to compare with data from two small, cleaner satellites, Skipper[8] and Atmosphere Explorer (AE)[1]; however, data are presently available from AE only. Almost all models of visible spacecraft glow attribute the glow to emission from excited NO_2 formed at the surface. These models have not resolved the question of the source of NO or addressed the magnitude of the glow as a function of altitude.

This paper examines the chemical reactions in the flowfield of a small satellite as one source of NO, the precursor to NO_2. Various neutral–neutral chemical reactions were incorporated in the direct simulation Monte Carlo (DSMC) modeling; however, the key shock layer chemical reaction for the formation of NO is the reaction of O with N_2. A DSMC method[9] that included gas-phase reactions of ambient gases to form NO under moderate to highly rarefied freestream conditions was used. Because the flow conditions are highly rarefied, the sensitivity of the model to freestream conditions was also considered. Without the benefit of the DSMC technique, numerical calculations would not be possible under these rarefied conditions.

For the conditions under consideration the number densities of nitric oxide and atomic nitrogen in the freestream are less than the number densities of other species in the freestream (N_2, O_2, and O) by several orders of magnitude. Also, the production rates of NO and N in the flowfield are very low due to the rarefaction effects. Thus, NO and N can be considered as trace species, and the standard DSMC technique must be modified. The proper representation of the trace species in the DSMC calculations requires an unacceptably large number of simulated particles in the flow domain, resulting in a massive computational effort. To handle these computational problems, a new DSMC technique has been developed and used for the present calculations. This new DSMC technique is conceptually similar to the Monte Carlo overlay method of Karipides et al.[7] but differs in the detailed implementation.

The incident rate of NO striking the surface can be calculated with the DSMC technique, and it will be shown that there is sufficient NO formed due to chemical reactions in the flowfield to assign it as a precursor to the glow. To quantitatively model the glow, a surface model must be developed for the conversion of NO to excited-state NO_2^*. (NO_2^* designates an electronic excited state of NO_2.) The present work models the surface reactions for the formation of excited NO_2 at the surface using the DSMC method[9] and, using a set of parameters to represent the surface conditions, calculates the radiance as a function of the orbit.

The outline of the paper is as follows: The main features of a surface model that are evaluated in a full DSMC simulation will be discussed in the next section. The key surface interactions and parameters will be introduced. Based on the most likely surface parameters for a spacecraft surface, the suggested mechanism is an Eley–Rideal model. The large variation in the surface and glow literature for the values of the fundamental surface parameters is discussed in this section as well. A set of initial values is suggested and modeled directly in the DSMC calculations for the formation of NO_2^* and the glow radiation. The computational method of calculating the formation of NO, as well as the inclusion of the surface processes into the DSMC calculations, and the results are discussed in the following section. The results of that section demonstrate the utility of an overlay technique in the calculations of trace species such as NO, the main precursor, and NO_2^*. The calculations will also show that it is possible to decouple the rarefied flow and gas/surface interactions, for the densities under consideration, which is useful if the dynamics of spacecraft glow are to be studied. A comparison of the calculated radiance with the AE data is given. The lack of satisfactory comparison suggests that both the surface parameters and processes must be reconsidered in the context of the actual satellite orbital parameters. Based on input from the DSMC calculations, the last section develops the full time-dependent glow equations that are directly applied to a low Earth orbit.

Surface Model for DSMC Simulations

The surface model assumes that the spacecraft is covered with at least a few layers of an oxide surface. The surface oxide layer

Received May 9, 1998; revision received Dec. 3, 1998; accepted for publication Dec. 7, 1998.

*Senior Research Engineer. Associate Fellow AIAA.
†Professor Emeritus, Department of Electrical Engineering.
‡Research Professor, Department of Chemistry. Member AIAA.

will be treated as being chemisorbed and not available to react with incoming NO. Additional surface bombardment by O and NO will result in those species being physisorbed to the surface. The principal process for surface glow follows an Eley–Rideal mechanism[10] with NO_2^* formed by collisions of O with surface-physisorbed NO. The formation of NO_2^* could potentially occur via a Langmuir–Hinshelwood mechanism involving the reaction of both surface adsorbed NO and O. This mechanism was not considered, based on the range of heat of adsorption values that are reasonable for a surface glow model. Gasser[10] provides an estimate of the number of surface sites a surface adsorbed species can visit based on its heat of adsorption. A low value of about four site hops and that the fractional coverage of surface adsorbed O will be shown to be very low make the Eley–Rideal mechanism a more realistic choice.

The physisorption process implies weaker bonding than chemisorption with a typical heat of absorption of about 5 kcal/mole (Ref. 11). However, there is not a sharp distinction between physisorption and weak chemisorption.[10] The term *physisorption* is used to describe the process where by NO is adsorbed without dissociation and with weak chemical bonding to the surface. The physisorption data suggest that NO has a larger bonding energy to a metal oxide surface than O (Ref. 11). A low bonding energy (~3–5 kcal/mole) for O will give a fractional coverage of adsorbed O too low for it to act as a major contributor in the production of NO_2^*. (Nevertheless, both processes will be carried in the test cases and DSMC code.) The measurements of Sonnenfroh and Caledonia[12] indicate that NO is bound to a laboratory Ni surface with approximately 6.5 kcal/mole. Recent thermal desorption spectra of NO on NiO(100)/Ni(100) and NO on a thin NiO(100) film show a heat of adsorption of about 10 kcal/mole (Ref. 13). Finally, the heat of adsorption of NO from bare Ni has been measured to be 23 kcal/mole (Ref. 14).

In the modeling, a value for the heat of adsorption is required. However, because the heat of adsorption depends on the surface material and its condition, there remains a large uncertainty in this parameter. The spacecraft glow intensity is directly proportional to the precursor-adsorbed species coverage, which in turn is sensitive to the heat of adsorption. The range of chemisorption energies is quite large, extending from about 10–195 kcal/mole (Ref. 15). Hence, to exercise the model two values for the heat of adsorption of NO, 10 and 20 kcal/mole, both within the range of weak chemisorption will be considered. The corresponding values for the heat of adsorption of O used were 10 and 3 kcal/mole.

The number of empty surface sites available for either O atom or NO molecule physisorption will be a function of the spacecraft altitude, the rates of surface adsorption and desorption, and other surface removal processes. During these processes, a monolayer of adsorbed species is formed at the oxide surface so that each site adsorbs at most one gas species. The surface processes can be expressed as

$$O + S \overset{k_1}{\longleftrightarrow} OS \tag{1}$$

$$NO + S \overset{k_2}{\longleftrightarrow} NOS \tag{2}$$

$$NO + OS \xrightarrow{\sigma_3} NO_2 + S + h\nu \tag{3}$$

$$O + NOS \xrightarrow{\sigma_4} NO_2 + S + h\nu \tag{4}$$

$$M + OS \xrightarrow{\sigma_{5M}} M + O \tag{5}$$

$$M + NOS \xrightarrow{\sigma_{6M}} M + NO \tag{6}$$

where S is a surface site available for physisorption and OS and NOS are those species adsorbed to the surface. The forward ($k_{f1,2}$) and backward ($k_{b1,2}$) reactions of Eqs. (1) and (2) represent adsorption and desorption, respectively. Surface adsorbed species may also be removed from the surface by collisions with the incoming flow gas species in two possible ways. Equations (3) and (4) represent the removal of an adsorbed species and the generation of radiation, whereas Eqs. (5) and (6) represent removal by a nonreactive processes, called here *scrubbing*. The scrubbing processes are assumed to involve the major gas species M, or N_2, O_2, and O, with the first two species assumed to be twice as efficient as O based on their larger masses, or $\sigma_{iN_2} = 2\sigma_i$, $\sigma_{i,O_2} = 2\sigma_i$, and $\sigma_{iO} = \sigma_i$, $i = 5, 6$. Specific values used for σ_5 and σ_6 will be discussed subsequently. Equations (3–6) are assumed to proceed only in the forward direction. Using Eqs. (1–6), the concentration of a surface species, e.g., NOS, can be expressed as

$$\frac{dn_{NOS}}{dt} = k_{f2} n_S f_{NO} - n_{NOS}\left(k_{b2} + \sigma_4 f_O + \sum_M f_M \sigma_{6M}\right) \tag{7}$$

where f_O and f_{NO}, are the fluxes of O and NO to the surface (number/m^2-s), n_{NOS} and n_{OS} are the surface number density (number/m^2) of NO and O adsorbed on the surface, and n_S is the number of (empty) surface sites available. The expression may be further reduced by assuming conservation of surface sites:

$$n_T = n_{OS} + n_{NOS} + n_S \tag{8}$$

where n_T is the total number of available surface sites per unit area.

The adsorption and desorption rate constants, $k_{f1,2}$ and $k_{b1,2}$, have been expressed in earlier DSMC work using transition state theory as[16]

$$k_{f1} = \frac{h^2 T}{2\pi m_a k \theta_D^2} \tag{9}$$

$$k_{b1} = \frac{k\theta_D}{h} \exp\left(-\frac{H_{os1}}{kT}\right) \tag{10}$$

where h is Planck's constant, k is the Boltzmann constant, m_a is the mass of atomic oxygen, H_{os1} is the heat of adsorption, θ_D is the debye temperature, and T is the surface temperature. Equations (9) and (10) are valid for the condition where the surface and gas phase are in thermochemical equilibrium at T. Because the flows of interest here are highly rarefied and in thermochemical nonequilibrium, the validity of this relationship can be questioned. Instead, a forward rate that is derived from the inherent properties of the gas species incident on the surface and the surface material, a sticking coefficient, was used. The sticking coefficient S_0 is then expressed in terms of $k_{f1,2}$ as

$$S_0 = k_{f1,2} n_T \tag{11}$$

where the $i = 1, 2$ subscript for S_0 has been suppressed because a common value is assumed. The work of Vattuone et al.[17] and Insepov and Zhankadamova[18] suggests a sticking coefficient of about 0.5. The use of a forward rate k_{f1}, derived from the sticking coefficient of 0.5 instead of a value derived from the expression given by Eq. (9), represents a significant departure from equilibrium conditions. If the same values were used in Eq. (9), i.e., $T = 300$ K and a debye temperature of 400 K, a rate of 3.6×10^{-22} m^2 would be obtained. However, when the sticking coefficient relationship is used, the absorption rate is found to be about two orders of magnitude higher, 2.1×10^{-20}. Equating the right-hand side of Eq. (9) to this value of 2.1×10^{-20} gives an effective translational temperature of 17,500 and not 300 K. This value of the temperature is appropriate to a beam of about 8-km/s species hitting the surface. After the species has hit the surface and stuck, it can then be assumed that the species has equilibrated with the wall temperature, and the value of 300 K can be used in Eq. (10) for the calculation of the desorption rate. For the calculations presented in this paper, a debye temperature of 400 K, a wall temperature of 300 K, and a total number of satellite surface sites of 0.24×10^{20} /m^2 (from purely geometric considerations) were assumed.

The second part of the surface model [Eqs. (3–6)] involves the reaction of physisorbed O and NO with the incoming NO and O gases to release the physisorbed species and form NO_2^*, which then emits a photon to the ground state, NO_2, or to scrub NO or O from the surface back into the gas phase. Quantitative measurements of these separate reactive and nonreactive cross sections have not been made, and a range of values will be inferred from experimental data and phenomenological evidence. The data of Baulch et al.[19] give a value for the three-body gas-phase process:

$$NO + O + M \xrightarrow{k_{3\text{-body}}} NO_2 + M \tag{12}$$

of $k_{3\text{-body}} = 3.0 \times 10^{-33}\ \exp(940/T)\text{cm}^6/\text{mol-s}$. Using simple gas kinetic theory, a methodology for relating gas–gas-phase interactions to surface-phase processes can be derived. In the gas phase, the reaction cross section for a binary process can be related to that of a tertiary process as

$$\sigma_{2\text{-body}} = n_c A_3 \frac{\lambda}{\bar{d}} \sqrt{\frac{\mu}{8\pi kT}} \tag{13}$$

where $\sigma_{2\text{-body}}$ is the reaction cross section for the two-body process, n_c is the concentration in number/cm^3 of the third body in the three-body gas-phase reaction [or M in Eq. (12)], A_3 is the Arrhennius coefficient for Eq. (12), λ is the mean free collision path, $\bar{d}$ is the average diameter of the species, and μ is the reduced mass. From the work of Sonnenfroh and Caledonia,[12] an approximate binding energy of 6.5 kcal/mole is given and can be compared with the gas-hase activation energy of Baulch et al.[19] of about 2 kcal/mole. Our surface of interest is not Ni, and the characterization of the spacecraft compared to the actual measurements of Sonnenfroh and Caledonia cannot be determined because the specific satellite surface material is not known. Therefore, to first order, the activation energy for the process for the formation of NO_2 is roughly the same in the surface and gas phases, as is consistent for physisorption processes. Accepting this connection, we can interpret the third body as the surface and $\sigma_{2\text{-body}}$ as the rate for the process:

$$O + NOS \xrightarrow{\sigma_{2\text{-body}}} NO_2$$

Typical numbers substituted into Eq. (13) give a value of $\sigma_{2\text{-body}}$ on the order of 1–10 Å^2.

In a similar manner, the gas-phase measurements of Fontijn et al.[20] of the rate constant for the production of NO_2^* can be used to estimate σ_4. From their measurements at 300 K, they found that the chemiluminescent (light-producing) process was about a factor of 1/30th as efficient as Eq. (12). Their rate for the chemiluminescent gas-phase process was also found to be about two orders of magnitude higher than that measured by Wurster and Marrone[21] at 3750 K and reevaluated by Baulch et al.[19] and Levitt.[22] The decrease in the rate at increased temperatures is attributed to the competition of processes that do not proceed through the $NO_2(\tilde{A})$ state, the precursor electronic state responsible for the visible glow, and the increased likelihood of populating higher vibrational–rotational levels of the $\tilde{A}$ state that predissociate. Hence, for the collision energies of interest here, the range of reasonable values for σ_4 is on the order of 1–0.001 Å^2, with a more likely value closer to 0.001 Å^2. It is interesting to point out that gas phase measurements of Fontijn et al.[20] also show that about one binary collision in 10^6 produces the emission of light. The gas-phase value will be shown to be similar to that observed in the spacecraft glow measurements and further encourages the model of a physisorbed or weakly chemisorbed NO surface species as a precursor to the spacecraft glow.

A value for the scrubbing cross sections [Eqs. (5) and (6)] is required. The measurements of Sonnenfroh and Caledonia[12] show a range of values with a maximum for the total collisional desorption cross section of 1.6 Å^2. We have considered a range of values of 0.01–1 Å^2 because it is unlikely that the process is truly gas kinetic and data on these specific processes are not readily available.

Finally, with the definition of the surface processes and estimates of the physical parameters, an expression for the glow radiation can be developed. For the AE geometry the observations were made looking through the glow. The total intensity I, in units of photon/cm^{2}s, can be expressed in terms of the spatial distribution of NO_2^*, designated as N^*, as

$$I = \int_0^{2\pi} \int_0^{\infty} \frac{1}{4\pi} \frac{N^*(x)}{\tau}\, \mathrm{d}x\, \mathrm{d}\Omega = \frac{1}{2} \int_0^{\infty} \frac{N^*(x)}{\tau}\, \mathrm{d}x \tag{14}$$

where τ is the radiative lifetime and $x = 0$ is the surface. Although the flow is highly rarefied, using a planar model we can estimate the distribution of the NO_2^* gaseous species in front of the surface in steady state as

$$\frac{\partial(N^* v)}{\partial x} = -\frac{N^*}{\tau} \qquad \text{or} \qquad N^*(x) = C_0 \exp\left(-\frac{x}{\tau v}\right) \tag{15}$$

The variable of integration C_0 is the value of $N^*(x = 0)$ and is equal to $\dot{N}_s^*/v$, where $\dot{N}_s^*$ is the generation rate of NO_2^* at the surface and v is the velocity of the gas. Substituting Eq. (15) into Eq. (14) gives

$$I = \frac{(\sigma_3 n_{NOS} f_O + \sigma_4 n_{OS} f_{NO})}{2} \tag{16}$$

An interesting result of Eq. (16) in the planar model is that the surface irradiance is independent of the lifetime of the radiating state. Thus, in this first-order analysis, we can see that the uncertainty of the lifetime due to surface effects is removed. Likewise, we would expect in the full DSMC calculation that the result would not be strongly influenced by the specific lifetime value. Reasonable comparison between the radiation calculated with the complete DSMC solution used in Eq. (14), and this approximation will demonstrate the utility of Eq. (16).

DSMC Computational Approach

To model a gas flow with infrequent collisions leading to the production of NO required a new DSMC technique, which is discussed here. In this new technique, the simulations are performed in two steps. First, the DSMC calculations are performed with a reasonable number of simulated particles so that the major species are represented appropriately in the computational domain. Then the second DSMC calculations are performed, where it is assumed that trace species particles do not affect the major species particles. Therefore, the number of major species-simulated particles, their positions in the flow domain, and their properties (based on previous calculations) remain unchanged. On the contrary, the simulated particles of trace species are increased so that they are represented properly in the flowfield and they are free to move in the flowfield. The flowfield has two different sets of simulated molecules: a major species set and a trace species set. The number of real molecules represented by a simulated particle is different in these two sets. Therefore, for the calculation of the number of collision pairs in the no time-counter routine, the major species simulated particles number is increased by multiplying a weighting factor so that a simulated particle of the major and trace species represents the same number of real molecules. In the pair selections, the major species simulated particles are also weighted accordingly. Thus, the right collision frequency is obtained, and there is no bias in species selection. Only those major–major species collisions that produce the trace species are accepted, and in these collisions, major species particles remain unchanged. Among the trace–trace species collisions, any formed major species particle is removed from the flowfield. In the case of the major–trace species particles collisions, any newly formed major species particle is also removed from the flowfield. In the collisional mechanics and chemistry routines, all particles have the same weighting factors. Otherwise, the standard DSMC collision mechanics is used for the collisions.

Gas–surface processes are evaluated concurrently with the calculation of the gas-phase flow. At each time step in the calculation of the major species, the rate equation for the physisorption of atomic oxygen at the surface,

$$\frac{\mathrm{d}n_{OS}}{\mathrm{d}t} = S_0 f_O \left(1 - \frac{n_{OS}}{n_T}\right) - k_{b1} n_{OS} \tag{17}$$

is solved numerically, based on the fluxes and occupied site values at the previous and present time steps using a Runge–Kutta method. Thus, the atomic oxygen particles that strike the surface in a time step are removed from the flowfield with the probability

$$P_{r1} = S_0[1 - (n_{OS}/n_T)] \tag{18}$$

and the number of simulated particles that are added (desorbed) in the flowfield from the surface per unit area in time Δt are equal to $k_{b1} n_{OS} \Delta t$. The calculations proceed until the flow reaches steady state and the flux of atomic oxygen to the surface and the atomic oxygen fractional surface coverage does not change.

In the trace species DSMC calculations, each time a simulated NO molecule strikes the surface it is checked to see whether it

has possibly participated in the process given by Eq. (3), with the probability given as

$$P_{r2} = \sigma_3 n_{OS} \tag{19}$$

If the NO particle is accepted for the reaction, then it is removed from the flowfield, and a NO_2^* simulated particle is added in the flowfield near the surface with the velocity according to the half-range equilibrium Maxwellian distribution based on the surface temperature. These NO_2^* particles move in the flowfield without any collision between themselves and other species; however, they can radiate in the flowfield with the specified radiation lifetime τ to decay to the ground electronic state of NO_2. At each time step, a test is performed for all of the existing NO_2^* particles. An acceptance–rejection method is used to test whether a particle will radiate. All particles are assumed to have equal probability of radiation, which is equal to $\Delta t/\tau$. Generally, the value of σ_3 is very small, which makes the reaction given by Eq. (3) for a simulated molecule of NO to become NO_2^* a rare event. Therefore, the probability as shown in Eq. (19) is increased by the multiplication of the weighting factor to obtain a reasonable sample size of reactions of simulated molecules. Each time a simulated NO molecule reacts at the surface to form a simulated NO_2^* molecule, according to a weighted probability, it is considered that only a fraction (1/weighting factor) of the simulated NO molecule has reacted. The fraction of reacted NO molecules is accumulated, and when it becomes unity, a simulated molecule of NO is removed from the flowfield. Hence, the NO_2^* simulated molecules formed at the surface contain (1/weighting factor) less number of real molecules as compared to real molecules represented by one simulated molecule of NO. Again, the calculations proceed until the flow reaches steady state and the flux of NO to the surface and the NO fractional surface coverage does not change.

After the first (major species) and second (trace species) sets of gas and surface calculations have reached steady state, a final set of simulations are performed. The third set of DSMC calculations is performed for major species again, where the reaction described by Eq. (4) is allowed at the surface by using the surface coverage values of NO calculated from the second set of DSMC calculations for trace species. Each time a simulated particle of atomic oxygen strikes the surface, it is checked to see whether it has participated in the reaction given by Eq. (4). The probability of a reaction is given as

$$P_{r3} = \sigma_4 n_{NOS} \tag{20}$$

and rest of the numerical technique used for the formation and destruction (radiation) of NO_2^* is the same as described in the trace species DSMC calculations.

In these calculations, a fine grid resolution is used for cells. The cell dimensions are much less than the local mean free path. A steady state is assumed when the number of simulated particles, including the newly formed particles at the surface in the flowfield, achieved a fixed value within statistical fluctuations. The final results are obtained through a time-averaged solution over a large number of time steps. In the steady state, the number of trace species particles per cell was on average 70. The statistical fluctuations in the computed macroscopic quantities (such as the NO surface flux) are on the order of 12%.

The molecular collisions are simulated by the variable hard sphere molecular model. Energy exchange between the translational and internal modes is modeled by the Larsen–Borgnakke statistical model[23] with rotational and vibrational collision numbers of 5 and 50, respectively.

The total collision energy model of Bird[24] has been used to simulate the chemical reactions in the flowfield, and 19 chemical reactions are considered for this study. The three-body reactions are not significant in the flowfield under the present conditions and are not included in the flowfield chemistry. The reaction rate data for the five-species air model (O_2, N_2, O, N, NO) (Table 1) are the same as those used in earlier research.[25] The data are derived from the compilation by Bortner.[26]

DSMC Simulation Results

Flowfield and Surface Fluxes

The flow conditions and the body configuration of the Skipper[8] satellite are used for the present calculations. The altitude range used is that from 130 to 200 km, which encompasses moderate to high rarefied conditions. A freestream velocity of 7.922 km/s is considered for these simulations. The freestream conditions for the major species are from Jacchia,[27] and those for the trace species are from a sounding rocket experiment.[28] The gas–surface interaction for those molecules that do not participate in the surface reactions is assumed to be diffuse with full thermal accommodation, and the surface temperature is assumed to be at a constant value of 300 K. Table 2 lists the freestream and flow conditions used in the calculations for this work.

A range of altitudes is investigated for the production of NO in the flowfield and formation of NO_2^* at the surface with a proposed surface model using DSMC axisymmetric calculations for the Skipper satellite configuration. Using the code, the production of NO in the axisymmetric flowfield and the formation of NO_2 at the surface were simulated. The geometry is shown in Fig. 1. A comparison of the flowfield and formation rates for the axisymmetric case (the Skipper geometry) and the cylindrical body (the AE geometry) was also carried out. The small differences found allowed a comparison of the AE data with the axisymmetric case for which more extensive calculations were performed. Figure 2 shows the computational grid used for the DSMC calculations to model the Skipper satellite environment, with a base diameter of 0.772 m and a nose radius of 1.0 m. It is reasonable to compare the results

Table 1 List of chemical reactions[a]

Reaction number	Reaction and energy, J	A	B	E_a/k, K
1	$O_2 + N + 8.197 \times 10^{-19} \rightarrow 2O + N$	5.993×10^{-12}	1	59,370
2	$O_2 + NO + 8.197 \times 10^{-19} \rightarrow 2O + NO$	5.993×10^{-12}	1	59,370
3	$O_2 + N_2 + 8.197 \times 10^{-19} \rightarrow 2O + N_2$	1.198×10^{-11}	1	59,370
4	$O_2 + O_2 + 8.197 \times 10^{-19} \rightarrow 2O + O_2$	5.393×10^{-11}	1	59,370
5	$O_2 + O + 8.197 \times 10^{-19} \rightarrow 2O + O$	1.498×10^{-10}	1	59,370
6	$N_2 + O + 1.561 \times 10^{-18} \rightarrow 2N + O$	3.187×10^{-13}	0.5	113,000
7	$N_2 + O_2 + 1.561 \times 10^{-18} \rightarrow 2N + O_2$	3.187×10^{-13}	0.5	113,000
8	$N_2 + NO + 1.561 \times 10^{-18} \rightarrow 2N + NO$	3.187×10^{-13}	0.5	113,000
9	$N_2 + N_2 + 1.561 \times 10^{-18} \rightarrow 2N + N_2$	7.968×10^{-13}	0.5	113,000
10	$N_2 + N + 1.561 \times 10^{-18} \rightarrow 2N + N$	6.900×10^{-8}	1.5	113,000
11	$NO + N_2 + 1.043 \times 10^{-18} \rightarrow N + O + N_2$	6.590×10^{-10}	1.5	75,550
12	$NO + O_2 + 1.043 \times 10^{-18} \rightarrow N + O + O_2$	6.590×10^{-10}	1.5	75,550
13	$NO + NO + 1.043 \times 10^{-18} \rightarrow N + O + NO$	1.318×10^{-8}	1.5	75,550
14	$NO + O + 1.043 \times 10^{-18} \rightarrow N + O + O$	1.318×10^{-8}	1.5	75,550
15	$NO + N + 1.043 \times 10^{-18} \rightarrow N + O + N$	1.318×10^{-8}	1.5	75,550
16	$NO + O + 2.719 \times 10^{-19} \rightarrow O_2 + N$	5.279×10^{-21}	−1.0	19,700
17	$N_2 + O + 5.175 \times 10^{-19} \rightarrow NO + N$	1.120×10^{-16}	0.0	37,500
18	$O_2 + N + 2.719 \times 10^{-19} \rightarrow NO + O$	1.598×10^{-18}	−0.5	3,600
19	$NO + N + 5.175 \times 10^{-19} \rightarrow N_2 + O$	2.490×10^{-17}	0.0	0

[a]Five-species model. Rate coefficient, $m^3/(mol\text{-}s) = AT^{-B} \exp(-E_a/kT)$.

Table 2 Freestream conditions

Altitude, km	Total number density $\times 10^{16}$, m^{-3}	Temperature, K	Mole fractions				
			$O_2 \times 10^{-2}$	N_2	O	$N \times 10^{-3}$	$NO \times 10^{-5}$
130	19.430	500	7.09	0.69	0.24	0.0	7
140	9.3540	625	6.18	0.65	0.29	0.05	8
150	5.3071	733	5.46	0.62	0.33	0.2	9
160	3.3508	822	4.86	0.58	0.37	1.04	11.0
180	1.6198	947	3.89	0.51	0.44	3.08	18.0
200	0.9061	1026	3.13	0.45	0.51	6.62	11.0

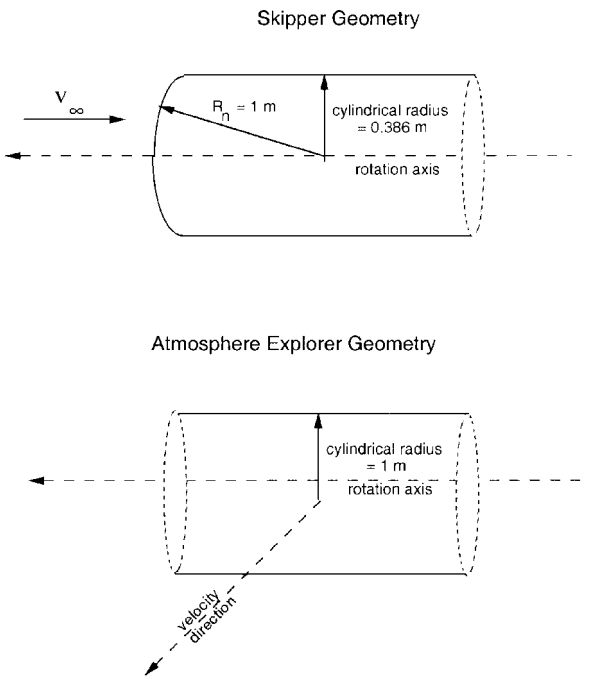

Fig. 1 Comparison of Skipper and AE.

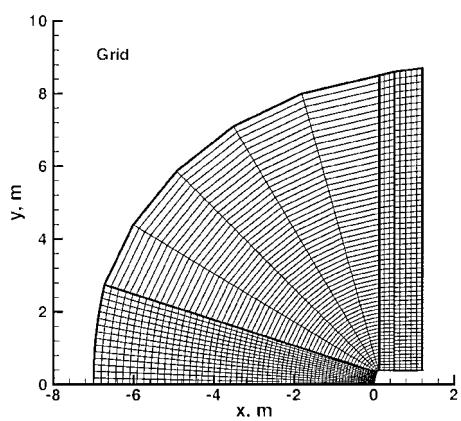

Fig. 2 DSMC computational grid of satellite.

for this geometry with AE data because both geometries have a nose radius of about 1.0 m, which is much less than the mean free path for all of the altitudes considered.

Figures 3 and 4 show the flowfield structure along the stagnation streamline for altitudes 130 and 160 km. The nondimensional density profiles in Fig. 3 show that shock wave is very diffuse for both altitudes, and a similar behavior has been observed for all of the altitudes considered. There is a large increase in the density near the stagnation point, which is characteristic of the flow at a cold wall for hypersonic conditions. The flowfield is rarefied for all

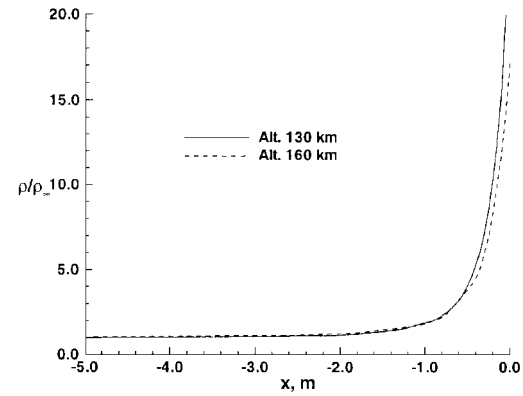

Fig. 3 Nondimensional density profiles along stagnation streamline.

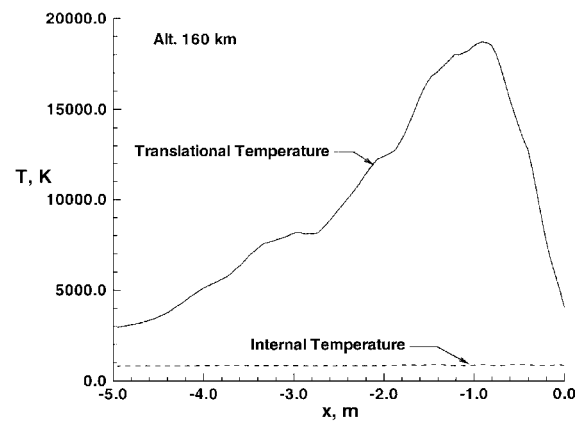

Fig. 4 Temperature profiles along stagnation streamline at 160 km.

of the altitudes considered, and the degree of rarefaction increases with increase in altitude. There is a considerable amount of thermal nonequilibrium in the flowfield because the internal and translational temperatures differ widely. The internal energy modes remain frozen at the freestream values due to the lack of collisions needed to excite these at rarefied conditions. This behavior is demonstrated in Fig. 4 for an altitude of 160 km.

For the modeling of surface-glow processes, an important parameter from the gas phase calculations is the flux of gas phase species toward the ram surface. The incident number flux (molecules striking the surface/m^2-s) at the surface for the various species is shown in Fig. 5 for 160 km. The incident fluxes are plotted as a function of the nondimensional distance (S/R_n) along the surface measured from the forebody stagnation point. The flow expansion at the corner reduces the fluxes to the side surface of the satellite as compared to the forebody surface. The relative surface flux values for different species, as well as the dependence with normalized surface distance, are similar for all altitudes considered. Figure 6 shows the altitude dependence of the surface fluxes at the stagnation point for the three major species (left-hand axis) and NO. All surface fluxes decrease

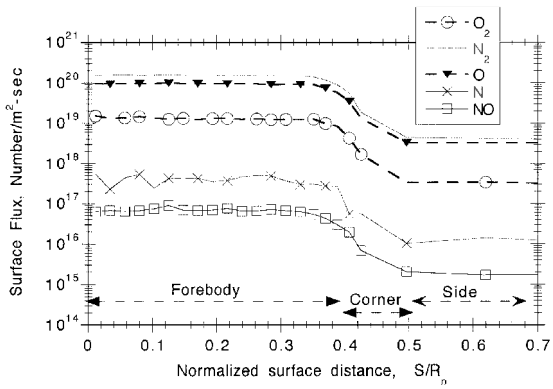

Fig. 5 Shock layer species surface flux profiles as a function of normalized surface distance at 160 km.

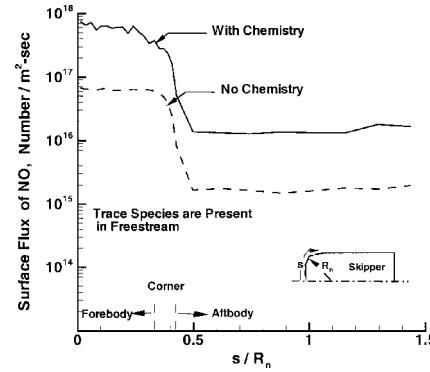

Fig. 7 Effect of chemistry on the surface incident number flux of NO at 140 km; note surface number flux is in the same units as used earlier.

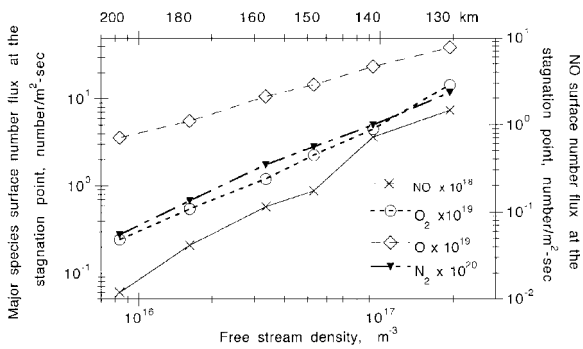

Fig. 6 Shock layer species surface flux at the stagnation point as a function of freestream number density.

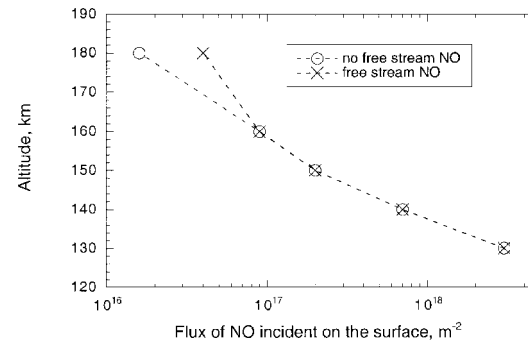

Fig. 8 Comparison of calculated NO flux levels incident at the surface as a function of altitude.

with increasing altitude, as expected, but not all species have the same density-dependent behavior. The lack of a simple density dependence is due to the change in the relative strength of the shock in front of the body for this altitude range. At higher densities, or increasing collision rates, the role of chemical reactions relative to the freestream conditions determines each species concentration. The altitude where these two effects are matched is different for each species. The number flux of molecular N_2 is much higher than the other species flux for all of the altitudes considered because it is the dominant species in the freestream. The surface number flux of atomic oxygen is higher at all altitudes than that of molecular oxygen. This is principally due to the larger number density of O than the O_2 in the freestream, although at lower altitudes the dissociation of O_2 also adds a small contribution. The surface flux of NO is about three orders of magnitude lower than that of the other species, consistent with the assumption that it is a trace species.

The density dependence of the NO surface flux is most important because it is a direct precursor to NO_2^*. The calculations show that the number density of NO, as well as the production rate of NO in the flowfield, decreases as the altitude increases. It can be observed in Fig. 6 that NO has the most pronounced change in its density dependence; hence, the mechanism for its production changes from high to low altitudes. Moreover, this change in density dependence is also seen in the AE radiance data. Figure 7 shows that at 140 km there is a considerable amount of NO production in the flowfield due to chemical reactions. The NO surface flux is shown for calculations with and without chemical reactions. At 140 km, chemical reactions provide more than an order of magnitude increase in the NO surface flux levels relative to the contribution of NO from the freestream. It has been observed from the calculations that the main reaction from Table 1 that contributes to the production of NO is $N_2 + O \rightarrow NO + N$. Figure 8 compares the computed NO incident surface flux at the stagnation point with and without NO present in the freestream. Figure 8 shows that for altitudes below 160 km the collision rate is sufficient to be the dominant source of NO. Even at 180 km, however, the inclusion of freestream NO only increases the NO surface flux level by a factor of about 2. Figure 8 also shows that the NO surface fluxes at higher altitudes will be affected by the high degree of variability of the ambient NO concentration. Because the ambient NO concentrations were not measured during AE, our modeled glow radiances at high altitudes will reflect this uncertainty as well.

The NO surface flux levels, although small, are sufficient to predict spacecraft glow. A radiative lifetime for NO_2^* can be estimated from the Shuttle observations, where the glow is observed to stand off about 10 cm from the body. A lifetime on the order of 0.3 ms is consistent with this observation and NO_2^* leaving the surface with a thermal velocity of the surface temperature (300 K) (Ref. 3). Use of this lifetime and the AE data permits an estimate of the number density of NO_2^*. Assuming that each NO produced in the gas phase strikes the surface and forms NO_2^*, our calculated NO flux levels are orders of magnitude higher than required by the AE data. However, the gas–surface conversion process will not occur with an efficiency of unity, and we now discuss results with the incorporation of a surface model.

Surface Simulation Results

To calculate the surface concentration of NO and O, the concentration of NO_2^*, and the radiation, the specific surface process cross sections must be given. Because the calculations reported in this section are primarily concerned with the demonstration of the DSMC computational technique, typical values were chosen. The second set of surface parameters used to explore a range of values that can be compared with data will be discussed in the subsequent section. The values selected here for the results shown in Figs. 9 and 10 were $H_{os1} = H_{os2} = 10$ kcal/mole, $S_0 = 0.5$, $\sigma_3 = \sigma_4 = 1$ Å^2, and $\sigma_5 = \sigma_6 = 0$. The choice of a scrubbing cross section of zero does not limit the demonstration of the method because the collisional removal rate is essentially attributed to the radiative channel only. Figure 9 shows contour levels for the NO_2^* concentration for 140 (top) and 180 (bottom) km. The gas density decreases at the higher altitude, and the majority of the excited states are produced in the

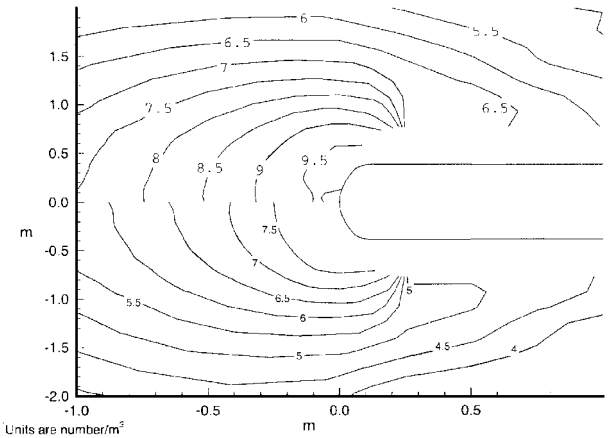

Fig. 9 Contour levels of $\log_{10}$ (NO_2^*) at 140 (top half) and 180 (bottom half) km for $H_{os1} = 10$ and $H_{os2} = 10$ kcal/mole.

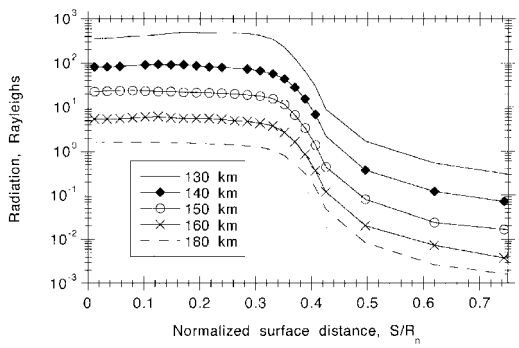

Fig. 10 Surface radiation as a function of altitude for $H_{os1} = 10$ and $H_{os2} = 10$ kcal/mole.

ram direction, consistent with the earlier surface flux plots. Using the tangent slab approximation to evaluate Eq. (14), the radiation at each point along the surface can be calculated. Figure 10 shows the radiance as a function of distance along the body using a lifetime of $\tau = 0.0003$ s and the DSMC-computed flow NO_2^* values.

To efficiently evaluate the change of radiance values for different surface parameters, it is important to assess the degree of coupling between the surface and the gas phase properties. The use of a physisorbed model and the highly rarefied nature of the flow suggest that at steady state changes in the properties of the adsorbed surface species do not influence the gas properties such as the flux incident to the surface. Figure 11 shows a comparison of the O and NO incident surface fluxes for the second set of heat of adsorption values that were considered, 20 kcal/mole for NO and 3 kcal/mole for O at an altitude of 160 km. Because the model assumes that the NO flux is produced by gas-phase reactions or freestream NO, the change in the heat of adsorption does not affect the incident surface fluxes. Furthermore, the model does not contain any surface catalytic values. Hence, the incident surface fluxes are invariant over this range of heat of adsorption values and flow conditions and need not be recalculated at each altitude for different adsorption values. The decoupling of the gas- and gas–surface-phase portions of the calculation is useful in the next section where a time-dependent, non-steady-state analysis is developed.

Surface Glow and Satellite Dynamics

The results of Fig. 10 show that a surface model can be incorporated into the DSMC formalism to evaluate surface reactions of trace species. Comparison of the stagnation point value at 140 km with the measured AE radiance value of approximately 60,000 Rayleighs[1] shows, however, that the present calculations substantially underpredict the data (Yee, private communication). This disagreement could be due to incorrect values for the surface fluxes (particularly NO), the surface model parameters, or both. A comparison of the

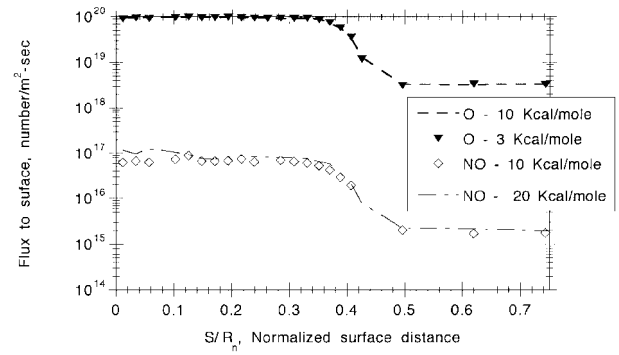

Fig. 11 Comparison of surface fluxes as a function of normalized surface distance for different heats of adsorption at 160 km; note that the NO and O surface fluxes calculated with the higher adsorption values are indicated by lines.

rate used for the production of NO with the recent trajectory calculations of Bose and Candler[29] shows that the latter rate may be higher, but the maximum difference is only about a factor of 5. Therefore, it is more likely that an improvement with data can be obtained by modifying the surface parameters.

Consider again the surface processes indicated in Eqs. (1–6). The concentration of NO and O adsorbed on the surface can be expressed as

$$\frac{\mathrm{d}n_{OS}}{\mathrm{d}t} = a_1 - b_1 n_{OS} - c_1 n_{NOS} \tag{21}$$

$$\frac{\mathrm{d}n_{NOS}}{\mathrm{d}t} = a_2 - b_2 n_{OS} - c_2 n_{NOS} \tag{22}$$

where the coefficients $a_{1,2}$, $b_{1,2}$, and $c_{1,2}$ are a function of time. The coupling in the equations occurs because the total number of surface sites (a constant) is the sum of the number of empty sites (available for adsorption) and the number with O and NO adsorbed. The last two terms are a function of time. It is instructive to look at the explicit form of Eq. (22). Use of Eqs. (10) and (11) gives

$$a_2 = S_0 f_{NO} \tag{23}$$

$$b_2 = (S_0/n_T) f_{NO} \tag{24}$$

$$c_2 = \frac{S_0 f_{NO}}{n_T} + \frac{k\theta_D}{h}\exp\left(-\frac{H_{os2}}{kT}\right) + f_O\sigma_4 + \sigma_6\left(f_O + 2f_{O_2} + 2f_{N_2}\right) \tag{25}$$

A similar set of relationships can be derived for a_1, b_1, and c_1. Setting the left-hand sides of Eqs. (22) and (21) to zero gives an explicit relationship for the steady-state values of n_{NOS} and n_{OS} in terms of the surface fluxes f_O, f_{NO}, f_{N_2}, and f_{O_2}, and the surface parameters. Figure 12 shows a comparison of the fractional surface coverage obtained from the steady-state solution of Eqs. (22–25) and the full DSMC calculation, for the same surface parameters used in the calculations shown in Figs. 9 and 10. The fractional surface coverage is the concentration of adsorbate divided by the total number of sites, e.g., n_{NOS}/n_T. Figure 12 shows again that the gas and gas–surface processes can be decoupled. The solution of Eqs. (22) and (21) for the surface concentrations, either in steady state or as a function of time, can be used in Eq. (16) to calculate the glow radiance. A comparison (not shown) of the stagnation point radiance values as a function of altitude computed with the full DSMC calculation and the use of Eqs. (16), (21), and (22) gave a factor of two agreement, which is much less than the other uncertainties in the surface model and is an indication of the accuracy of the approximations used in the particle–surface interaction simulation. (Note that for this choice of surface parameters the steady-state and time-dependent solutions are identical.) Hence, the remaining surface glow results are calculated using the decoupled DSMC-surface time-dependent model.

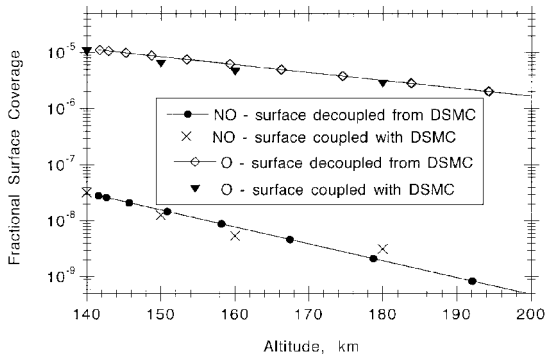

Fig. 12 Comparison of fractional surface coverage computed by DSMC and uncoupled steady-state solution for $H_{os1} = 10$ and $H_{os2} = 10$ kcal/mole.

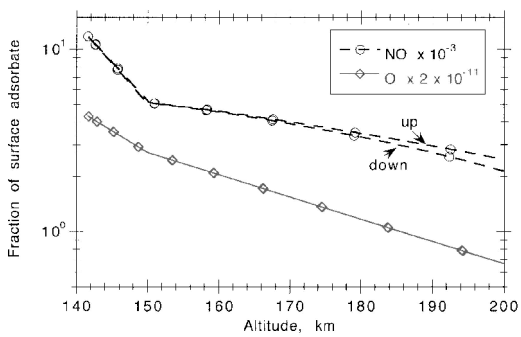

Fig. 13 Adsorbate fractional coverage for an AE orbit as a function of altitude.

Figures 10 and 12 suggest that the choice of typical surface parameters does not produce sufficient radiation because the fractional surface coverage is too low. Based on this test case, an increase in the surface concentration of NO is required. Equation (25) shows that the NO surface concentration can be significantly enhanced by increasing H_{os2}. Based on the earlier discussion of the range of reasonable surface parameters, we have chosen a second value of H_{os2} of 20 kcal/mole. (In addition, a more realistic value for the heat of adsorption of O to a metal oxide surface of 3 kcal/mole is assumed.) In the selection of the second set of surface parameters, we also considered a nonzero scrubbing cross section. However, an increase in the scrubbing cross section $\sigma_{5,6}$ decreases the amount of surface adsorbate and, therefore, reduces the radiation.

The surface fluxes, which have been shown as a function of altitude, become a function of time when associated with a specific satellite trajectory. The AE data examined in this paper correspond to orbit 1202, an elliptical orbit with a perigee of approximately 142 km and an apogee of about 4000 km.§ The surface adsorbate concentrations are calculated solving Eqs. (22) and (21) numerically with a Gear integration routine for stiff, coupled linear differential equations.[30] The integrations start at an altitude sufficiently high such that it can be assumed that the surface concentrations are initially zero and continue through the perigee and back up toward the apogee. Figure 13 shows the results of the time-dependent solution, and the values of the other surface parameters used in the calculations are $\sigma_3 = \sigma_4 = 0.01$ Å^2 and $\sigma_5 = \sigma_6 = 0.1$ Å^2. Two new features in the results are apparent. The NO adsorbate fractional surface concentration has increased by two orders of magnitude. With this value of H_{os1}, the NO surface concentration is not symmetric about the perigee, 142 km altitude. The surface NO concentration is higher after the perigee, upwards bound. The discontinuity in the surface adsorbate fraction reflects the changes in density dependence of the surface fluxes shown in Fig. 6.

The asymmetry in the calculated surface coverage means that the predicted glow radiance will also be asymmetric. It occurs primarily

§Mark Burrage, University of Michigan, http://www.sprl.umich.edu/VAE/.

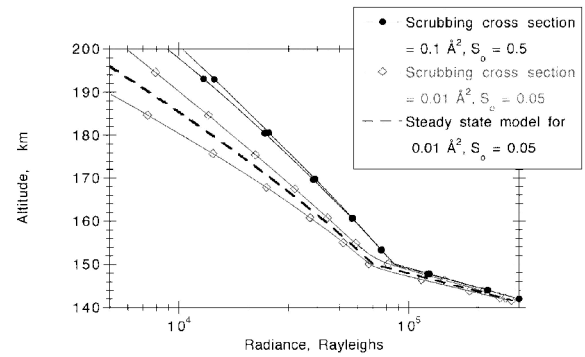

Fig. 14 Effect of time radiance solutions for different collisional removal cross sections; value of $\sigma_4 = 0.01$ Å^2 was used for both cases.

because the heat of adsorption is sufficiently large such that the surface lifetime begins to approach the rate of change of the surface fluxes about the orbit. The gas–surface-phase processes no longer remain in steady state with the local orbital conditions. The gas-phase processes, however (which determine the surface fluxes), reach steady state on the order of milliseconds, a much faster timescale. A value of 20 kcal/mole adsorption heat is approximately the lowest value that will induce an asymmetry in surface coverage for this orbit. In addition, the degree of asymmetry depends on the ratio of the two dominant terms in Eq. (25):

$$k\theta_D/h \exp[-(H_{os2}/kT)], \qquad \sigma_6\left(f_O + 2f_{O_2} + 2f_{N_2}\right)$$

Figure 14 shows that the asymmetry increases as the collisional removal (or scrubbing) cross sections are decreased or as the two terms approach comparable magnitudes. Again, higher values in the surface coverage or radiance are observed on the up-bound portion of the orbit. The change in S_0 does not change the shape of the time-dependent solution; rather, it is a constant scaling factor (in the a_2 term) enabling the two solutions to be plotted on a common set of axes. The steady-state solution for the lower scrubbing cross section is readily seen to be different from its corresponding time-dependent solution. Moreover, the asymmetry would be inconvenient to model in the surface-coupled DSMC solution because the latter calculation is carried out to steady state.

The present AE glow data are sufficiently convolved with background air glow that we are presently not able to correct for the variation of air glow during different parts of the orbit. Other data sets are presently under examination. However, we cannot use this data set to confirm or deny the existence of an asymmetry. If such data were available they would help to discriminate between the two surface models used in Fig. 14. The parameters used in the first case, $S_0 = 0.5$ and $\sigma_6 = 0.1$ Å^2, are closer to the values found in the literature and will be retained as our best estimate.

Finally, in Fig. 15 we compare AE orbit 1202 data with our calculations. The data values that we use in Fig. 15 are obtained from the work of Yee and Abreu[1] and are the in-band radiance measured in the 732 ± 2 nm photometer with the following modifications: To represent the total NO_2^* emission, the AE data must be increased by the ratio of the NO_2^* spectral distribution to the 2-nm spectral filter width. From the Shuttle glow spectral data,[2] we obtained an effective bandwidth of 249.8 nm for the NO_2^* emission. More recent considerations of the calibration methods used to reduce the AE data suggest a reduction of the original data given by Yee and Abreu[1] by a factor of 3 (Yee, private communication). The first set of calculations shown (diamonds) are identical to those shown in Fig. 14 (filled circles), and it is assumed that all species contribute to the scrubbing mechanism. Figure 15 shows that the absolute magnitude of these calculations is in much better agreement with the data than those calculations that used a heat of adsorption of 10 kcal/mole. Although the calculated radiance is higher than the data, the disagreement can be corrected within the choice of literature estimates for the radiation efficiency. A number of researchers have estimated the efficiency of the glow process. Mende et al.[31] approximates the Shuttle glow efficiency to be about 1 in 10^5 O particles. If we take

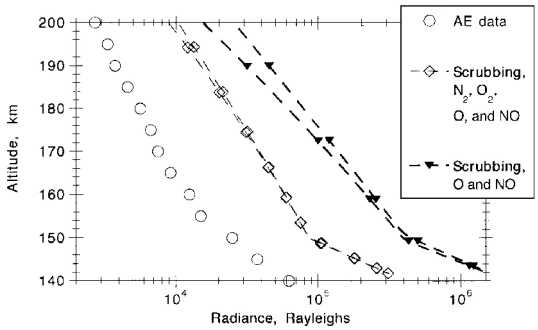

Fig. 15 Comparison of time-dependent radiance solutions with AE orbit 1202 data; value of $S_0 = 0.5, H_{os1} = 3, H_{os2} = 20$ kcal/mole, $\sigma_3 = \sigma_4 = 0.01$, and $\sigma_5 = \sigma_6 = 0.1$ Å^2 was used for all calculations.

the ratio of the AE radiance data to our computed O fluxes, we obtain an efficiency of about 1.5×10^{-6}–2.2×10^{-6}, which is close to what was observed in gas phase measurements of Fontijn et al.[20] and is closer to the glow efficiencies derived by Yee and Dalgarno.[32] Moreover, if we reexpress Eq. (16) as

$$\sigma_4 \approx \frac{2I_{\mathrm{AE}}}{n_{\mathrm{NOS}} f_{\mathrm{O}}}$$

and use our calculated adsorbed NO concentrations, we find that a value of 0.006 Å^2 brings us into agreement with the AE data. This is well within the range of cross sections estimated for this process. The sensitivity of our results to the inclusion of scrubbing by two of the major species, N_2 and O_2, is shown in the second calculation of Fig. 15. In that calculation (inverted triangles) the surface coverage increases, and similarly to Fig. 14 the time asymmetry is more apparent. The theory of Yang et al.[33] suggests these two species are as effective scrubbers as O or NO. Hence, when all of the surface fluxes are included, the surface coverage and radiance is reduced, the discontinuity in radiation is observed, and a small time asymmetry is predicted.

Conclusions

Our work on the topic of spacecraft glow has been conducted in two phases. The first phase of the work sought to identify the origin of the precursor species related to the glow. A new DSMC method suitable for trace species flowfield calculations, which includes chemical reactions, was developed and used for modeling a small satellite environment. That work identified NO formed in the bow shock in the ram direction of the spacecraft as the source of the glow mechanism. It was shown that the trace amounts of NO formed by the reaction of O and N_2 in the diffuse bow shock are adequate to provide the concentration of NO_2 observed in the AE data. Our results are similar to those obtained earlier by Karipides et al.,[7] who showed that a reasonable agreement between the freestream density dependence of the incident NO surface flux and the AE radiance is obtained. A simple freestream density dependence for the glow is not observed due to the changing contributions of freestream NO and that formed in the chemistry shock layer. Below 160 km, the NO formed in the shock layer is the dominant source.

The second phase of the work was to postulate and develop a surface model so that the radiance could be predicted in an absolute sense. The surface model presented here, based on an Eley–Rideal mechanism, assumes that a surface, physisorbed (weakly chemisorbed) NO molecule originally formed in the bow shock can stick to a metal-oxide surface, for a residence time on the order of 10–20 s and is subsequently removed by an incoming O atom to radiate or is collisionally removed from the surface without producing light. When evaluated with reasonable values for the heat of adsorption, a radiation cross section, and a collisional scrubbing cross section, the model gives good agreement with the absolute magnitude and shape of the AE data.

Acknowledgments

This research was supported by the Innovative Science and Technology Directorate of the Ballistic Missile Defense Organization (BMDO), Air Force Office of Scientific Research. Research performed at the Institute for Defense Analyses was carried out under Contract DASW01-94-C-0054 for BMDO. We would like to acknowledge the computer support received from Steven Taylor. We would further like to acknowledge the many useful discussions and the January 1998 private communication with J. H. Yee of the Applied Physics Laboratory.

References

[1]Yee, J. H., and Abreu, V. J., "Visible Glow Induced by Spacecraft–Environment Interaction," *Geophysical Research Letters*, Vol. 10., No. 2, 1983, pp. 126–129.

[2]Caledonia, G. E., Holtzclaw, K. W., Green, B. D., and Krech, R. H., "Laboratory Investigation of Shuttle Glow Mechanism," *Geophysical Research Letters*, Vol. 17, No. 11, 1990, pp 1881–1884.

[3]Caledonia, G. E., Holtzclaw, K. W., Krech, R. H., Sonnenfroh, D. M., Leone, A., and Blumberg, W. A. M., "Mechanistic Investigations of Shuttle Glow," *Journal of Geophysical Research*, Vol. 98, No. A3, 1993, pp. 3725–3730.

[4]Viereck, R. A., Murad, E., Pike, C. P., Mendes, S., Swenson, G., Culberston, S. L., and Springer, R. C., "Special Characteristics of the Shuttle Glow," *Geophysical Research Letters*, Vol. 19, No. 12, 1992, pp. 1219–1222.

[5]Orient, O. J., and Murad, E., "Recombination of 5-eV O(^3P) Atoms on Surface Adsorbed NO," *Physical Review A*, Vol. 45, No. 51, 1992, pp. 2998–3003.

[6]Swenson, G. R., Mende, S. B., and Clifton, K. S., "Ram Vehicle Glow Spectrum: Implications of NO_2 Recombination," *Geophysical Research Letters*, Vol. 12, 1985, pp. 97–100.

[7]Karipides, D. P., Boyd, I. D., and Caledonia, G. E., "Development of a Monte Carlo Overlay Method with Application to Spacecraft Glow," *Journal of Thermophysics and Heat Transfer*, Vol. 12, 1998, pp. 30–37.

[8]Levin, D., Finke, R., Candler, G., Boyd, I., Howlett, L., and Erdman, P., "In-Situ Measurements of Transitional and Continuum Flow UV Radiation from Small Satellite Platforms," AIAA Paper 94-0248, Jan. 1994.

[9]Bird, G. A., *Molecular Gas Dynamics and the Direct Simulation of Gas Flows*, Clarendon, Oxford, England, UK, 1994.

[10]Gasser, R. P. H., *An Introduction to Chemisorption and Catalysis by Metals*, Clarendon, Oxford, England, UK, 1985.

[11]Somorjai, G. A., *Principles of Surface Chemistry*, Prentice–Hall, Englewood Cliffs, NJ, 1972.

[12]Sonnenfroh, D. M., and Caledonia, G. E., "Collisional Desorption of NO by Fast O Atoms," *Journal of Geophysical Research*, Vol. 98, No. A12, 1993, pp. 21,605–21,610.

[13]Kuhlenbeck, H., Odörfer, G., Jaeger, R., Illing, G., Menges, M., Mull, T., Freund, H. J., Pöhlchen, M., Staemmler, V., Witzel, S., Scharfschwerdt, K., Wennemann, K., Liedtke, T., and Neumann, M., "Molecular Adsorption on Oxide Surfaces: Electronic Structure and Orientation of NO on NiO(100)/Ni(100) and on NiO(100) as Determined from Electron Spectroscopies and *Ab Initio* Cluster Calculations," *Physical Review B*, Vol. 43, No. 3, 1991, pp. 1969–1986.

[14]Hamza, A. V., Ferm, P. M., Budde, F., and Ertl, G., "The Dynamics of NO Scattering from NO- and CO-Covered Ni(100)," *Surface Science*, Vol. 199, 1988, pp. 13–27.

[15]Prutton, M., *Introduction to Surface Physics*, Oxford Science, Clarendon, Oxford, England, UK, 1994.

[16]Bergemann, F., "A Detailed Surface Chemistry Model for the DSMC Method," *Rarefied Gas Dynamics: Proceedings of the 19th International Symposium*, edited by J. Harvey and G. Lord, Oxford Univ. Press, Oxford, England, UK, 1995, pp. 947–953.

[17]Vattuone, L., Rocca, M., Boragno, C., and Valbusa, U., "Initial Sticking Coefficient of O_2 on Ag(110)," *Journal of Chemical Physics*, Vol. 101, No. 1, 1994, pp. 713–725.

[18]Insepov, Z. A., and Zhankadamova, A. M., "Molecular Dynamics Calculation of the Sticking Coefficient of Gases to Surfaces," *Z. Phys. D-Atoms, Molecules and Clusters*, Vol. 20, 1991, pp. 145–146.

[19]Baulch, D. L., Drysdale, D. D., Home, D. G., and Lloyd, A. C., *Evaluated Kinetic Data for High Temperature Reactions, 2, Homogeneous Gas Phase Reactions of the H_2-N_2-O_2 System*, Butterworths, London, 1972.

[20]Fontijn, A., Meyer, C. B., and Schiff, H. I., "Absolute Quantum Yield Measurements of the NO-O Reaction and its Use as a Standard for Chemiluminescent Reactions," *Journal of Chemical Physics*, Vol. 40, No. 1, 1964, pp. 64–70.

[21]Wurster, W. H., and Marrone, P. V., Cornell Aeronautical Lab., Rept. QM-1373-A-4, Cornell Univ., Ithaca, NY.

[22]Levitt, B. P., *Discussions of the Faraday Society*, Vol. 37, 1964, p. 222.

[23]Borgnakke, C., and Larsen, P. S., "Statistical Collision Model for Monte Carlo Simulation of Polyatomic Gas Mixture," *Journal of Computational Physics*, Vol. 18, No. 4, 1975, pp. 405–420.

[24]Bird, G. A., "Simulation of Multi-Dimensional and Chemically Reacting Flows," *Rarefied Gas Dynamics*, Vol. 1, edited by R. Campargue,

Commissariat a l'Energie Atomique, Paris, 1979.

[25]Moss, J. N., Bird, G. A., and Dogra, V. K., "Nonequilibrium Thermal Radiation for an Aeroassist Flight Experiment Vehicle," AIAA Paper 88-0081, Jan. 1988.

[26]Bortner, M. H., "Suggested Standard Chemical Kinetics for Flow-Field Calculations—A Consensus Opinion," *AMRAC Proceedings*, Vol. 14, Pt. 1, Doc. No. 4613-135-X, Inst. of Science and Technology, Univ. of Michigan, Ann Arbor, MI, April 1966, pp. 569–581.

[27]Jacchia, L. C., "Thermospheric Temperature, Density, and Composition: New Models," *Research in Space Science*, SAO Special Rept. 375, March 1977.

[28]McCoy, R. P., "Thermospheric Nitrogen 1. NO, N(^4S), and O(^3P) Densities from Rocket Measurements of the NO δ and γ Bands and the O_2 Herzberg I Bands," *Journal of Geophysical Research*, Vol. 88, No. A4, 1983, pp. 3197–3205.

[29]Bose, D., and Candler, G. V., "Simulation of Hypersonic Flows Using a Detailed Nitric Oxide Formation Model," *Physics of Fluids*, Vol. 9, No. 4, 1997, pp. 1171–1181.

[30]Kahaner, D., Moler, C., and Nash, S., *Numerical Methods and Software*, Prentice–Hall, Englewood Cliffs, NJ, 1989.

[31]Mende, S. B., Banks, P. M., and Klingelsmith, D. A., "Observation of Orbiting Vehicle Induced Luminosities on the STS-8 Mission," *Geophysical Research Letters*, Vol. 11, No. 5, 1984, pp. 527–530.

[32]Yee, J. H., and Dalgarno, A., "Radiative Lifetime Analysis of the Shuttle Optical Glow," *Journal of Spacecraft and Rockets*, Vol. 23, No. 6, 1986, pp. 635–640.

[33]Yang, K., Cheng, H., Vilallonga, E., and Rabitz, H., "Mechanisms of Collision-Induced Desorption of a Physisorbed Atom at Superthermal Energy: A Multiple Scattering Study," *Surface Science*, Vol. 326, 1995, pp. 177–194.

J. P. Gore
Associate Editor